The LABOCA Survey of the Extended *Chandra* Deep Field South: Clustering of submillimetre galaxies

Ryan C. Hickox[1,2,3]⋆, J. L. Wardlow[1,4], Ian Smail[5], A. D. Myers[6], D. M. Alexander[1],
A. M. Swinbank[5], A. L. R. Danielson[5], J. P. Stott[1], S. C. Chapman[7], K. E. K. Coppin[8],
J. S. Dunlop[9], E. Gawiser[10], D. Lutz[11], P. van der Werf[12], A. Weiß[13]

[1]*Department of Physics, Durham University, South Road, Durham DH1 3LE*
[2]*STFC Postdoctoral Fellow*
[3]*Department of Physics and Astronomy, Dartmouth College, 6127 Wilder Laboratory, Hanover, NH 03755, USA*
[4]*Department of Physics & Astronomy, University of California, Irvine, CA 92697, USA*
[5]*Institute for Computational Cosmology, Durham University, South Road, Durham DH1 3LE*
[6]*Department of Physics and Astronomy, University of Wyoming, Laramie, WY 82071, USA*
[7]*Institute of Astronomy, Madingley Road, Cambridge CB3 0HA*
[8]*Department of Physics, McGill University, Ernest Rutherford Building, 3600 Rue University, Montreal, Quebec H3A 2T8, Canada*
[9]*Institute for Astronomy, University of Edinburgh, Royal Observatory, Edinburgh EH9 3HJ*
[10]*Department of Physics and Astronomy, Rutgers, The State University of New Jersey, Piscataway, NJ 08854, USA*
[11]*Max-Planck-Institut für extraterrestrische Physik, Postfach 1312, 85741 Garching, Germany*
[12]*Leiden Observatory, Leiden University, NL 2300 RA Leiden, The Netherlands*
[13]*Max-Planck-Institut für Radioastronomie, Auf dem Hügel 69, 53121, Bonn, Germany*

5 December 2011

ABSTRACT

We present a measurement of the spatial clustering of submillimetre galaxies (SMGs) at $z = 1$–3. Using data from the 870 μm LABOCA submillimetre survey of the Extended *Chandra* Deep Field South, we employ a novel technique to measure the cross-correlation between SMGs and galaxies, accounting for the full probability distributions for photometric redshifts of the galaxies. From the observed projected two-point cross-correlation function we derive the linear bias and characteristic dark matter halo masses for the SMGs. We detect clustering in the cross-correlation between SMGs and galaxies at the $> 4\sigma$ level. Accounting for the clustering of galaxies from their autocorrelation function, we estimate an autocorrelation length for SMGs of $r_0 = 7.7^{+1.8}_{-2.3} \ h^{-1}$ Mpc assuming a power-law slope $\gamma = 1.8$, and derive a corresponding dark matter halo mass of $\log(M_{\mathrm{halo}}[h^{-1} \ M_\odot]) = 12.8^{+0.3}_{-0.5}$. Based on the evolution of dark matter haloes derived from simulations, we show that that the $z = 0$ descendants of SMGs are typically massive ($\sim$2–3 L^*) elliptical galaxies residing in moderate- to high-mass groups ($\log(M_{\mathrm{halo}}[h^{-1} \ M_\odot]) = 13.3^{+0.3}_{-0.5}$). From the observed clustering we estimate an SMG lifetime of $\sim$100 Myr, consistent with lifetimes derived from gas consumption times and star-formation timescales, although with considerable uncertainties. The clustering of SMGs at $z \sim 2$ is consistent with measurements for optically-selected quasi-stellar objects (QSOs), supporting evolutionary scenarios in which powerful starbursts and QSOs occur in the same systems. Given that SMGs reside in haloes of characteristic mass $\sim 6 \times 10^{12}$ $h^{-1} \ M_\odot$, we demonstrate that the redshift distribution of SMGs can be described remarkably well by the combination of two effects: the cosmological growth of structure and the evolution of the molecular gas fraction in galaxies. We conclude that the powerful starbursts in SMGs likely represent a short-lived but universal phase in massive galaxy evolution, associated with the transition between cold gas-rich, star-forming galaxies and passively evolving systems.

Key words: galaxies: evolution – galaxies: high-redshift – galaxies: starburst – large-scale structure of the Universe – submillimetre.

⋆ E-mail: ryan.c.hickox@dartmouth.edu

arXiv:1112.0321v1 [astro-ph.GA] 1 Dec 2011

1   INTRODUCTION

Submillimetre galaxies (SMGs) are a population of high-redshift ultraluminous infrared galaxies (ULIRGs) selected through their redshifted far-infrared emission in the submillimetre waveband (e.g., Smail, Ivison & Blain 1997; Barger et al. 1998; Hughes et al. 1998; Blain et al. 2002). The redshift distribution of this population appears to peak at $z \sim 2.5$ (e.g., Chapman et al. 2003, 2005; Wardlow et al. 2011), so that SMGs are at their commonest around the same epoch as the peak in powerful active galactic nuclei (AGN) and specifically quasi-stellar objects (QSOs) (e.g., Richards et al. 2006; Assef et al. 2011). This correspondence may indicate an evolutionary link between SMGs and QSOs, similar to that suggested at low redshift between ULIRGs and QSOs by Sanders et al. (1988). However there is little direct overlap ($\sim$ a few percent) between the high-redshift SMG and QSO populations (e.g., Page et al. 2004; Chapman et al. 2005; Stevens et al. 2005; Alexander et al. 2008; Wardlow et al. 2011). The immense far-infrared luminosities of SMGs are widely believed to arise from intense, but highly-obscured, gas-rich starbursts (e.g., Greve et al. 2005; Alexander et al. 2005; Pope et al. 2008; Tacconi et al. 2006, 2008; Ivison et al. 2011), suggesting that they may represent the formation phase of the most massive local galaxies: giant ellipticals (e.g., Eales et al. 1999; Swinbank et al. 2006).

SMGs and QSOs may thus represent phases in an evolutionary sequence that eventually results in the population of local massive elliptical galaxies. This is a compelling picture, but testing the evolutionary links is challenging due to the lack of an easily-measured and conserved observable to tie the various populations together. For example, the stellar masses of both QSOs and SMGs are difficult to measure reliably due to either the brightness of the nuclear emission in the QSOs (e.g., Croom et al. 2004; Kotilainen et al. 2009) or strong dust obscuration and potentially complex star-formation histories for the SMGs (e.g., Hainline et al. 2011; Wardlow et al. 2011; but see also Dunlop 2011; Michałowski et al. 2011), while the details of the high-redshift star formation that produced local massive elliptical galaxies are likewise poorly constrained (e.g., Allanson et al. 2009). Deriving dynamical masses for QSO hosts from rest-frame optical spectroscopy is difficult due to the very broad emission lines from the AGN, while dynamical mass measurements using CO emission in gas-rich QSOs are also challenging, due to the potential non-isotropic orientation of the QSO hosts on the sky and the lack of high-resolution velocity fields necessary to solve for this (Coppin et al. 2008), as well as the general difficulties in modeling CO kinematics (e.g., Tacconi et al. 2006; Bothwell et al. 2010; Engel et al. 2010).

Another possibility is to compare source populations via the masses of their central black holes. For QSOs and the population of SMGs that contain broad-line AGN, the black hole mass can be estimated using virial techniques based on the broad emission lines (e.g., Vestergaard 2002; Peterson et al. 2004; Vestergaard & Peterson 2006; Kollmeier et al. 2006; Shen et al. 2008). Such studies generally find that SMGs have small black holes relative to the local black hole-galaxy mass relations (e.g., Alexander et al. 2008; Carrera et al. 2011), while the black holes in $z \sim 2$ QSOs tend to lie above the local relation, with masses similar to those in local massive ellipticals (e.g., Decarli et al. 2010; Bennert et al. 2010; Merloni et al. 2010). These results suggest that SMGs represent an earlier evolutionary stage, prior to the QSO phase in which the black hole reaches its final mass. However, high-redshift virial black hole mass estimates are highly uncertain (e.g.,
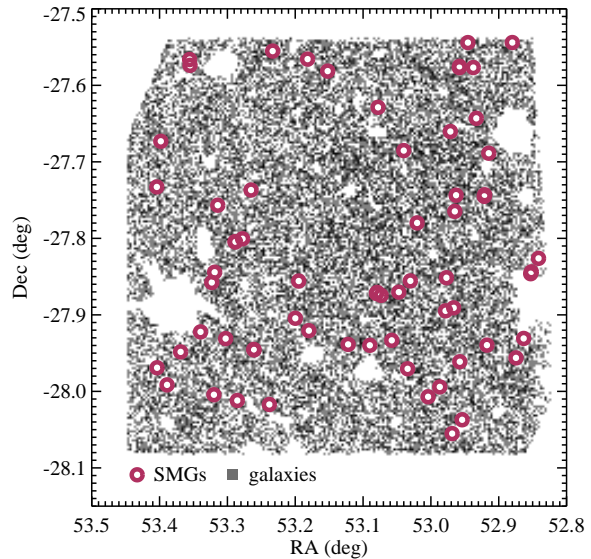

Figure 1. Two-dimensional distribution of the 50 LESS SMGs and $\sim$ 50,000 IRAC galaxies in the ECDFS that are used in our analysis. The SMGs shown represent the subset of the 126 SMGs in the full LESS sample (Weiß et al. 2009) that are in the redshift range $1 < z < 3$ and are in regions of good photometry, and so are used in this analysis. The IRAC galaxies are chosen to reside at $0.5 < z < 3.5$. The SMGs are shown here individually, while the density of galaxies is given by the grayscale. The blank areas represent regions which are excluded from the analysis, including areas of poor photometry (for example around bright stars) or additional sources identified by eye in the vicinity of SMG, as discussed in §2. The high density of IRAC galaxies in the field enables an accurate measurement of the SMG-galaxy cross-correlation function.
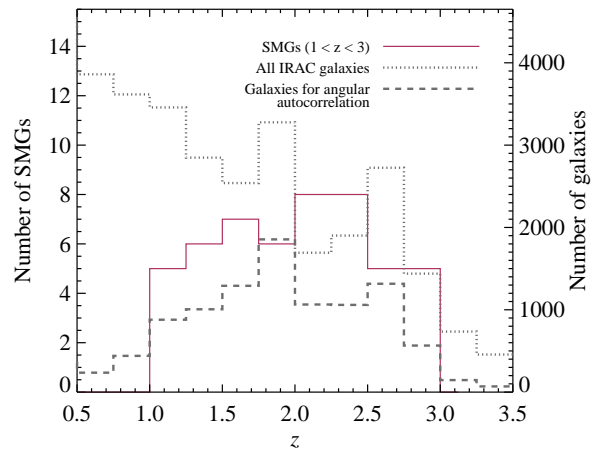

Figure 2. Redshift distributions for the IRAC galaxy sample in the redshift range $0.5 < z < 3.5$ (dotted line), and the SMG sample in the range $1 < z < 3$ (solid line). The histogram for galaxies has been scaled so that the distribution can be directly compared to that of the SMGs. Also shown is the redshift distribution for 11,241 galaxies (dashed line) selected to match the overlap in the redshift distributions of the SMGs and galaxies, as used in the galaxy autocorrelation measurement (§3.2). For the SMGs, 44% have spectroscopic redshifts, while the remainder of the SMGs and all the IRAC galaxies have redshift estimates from photometric redshift calculations (Wardlow et al. 2011).

Marconi et al. 2008; Fine et al. 2010; Netzer & Marziani 2010) and may suffer from significant selection effects (e.g., Lauer et al. 2007; Shen & Kelly 2010; Kelly et al. 2010), and so conclusions about connections between populations are necessarily limited.

The difficulties discussed above lead us to take another route to compare SMGs to high-redshift QSOs and low-redshift ellipticals: through their clustering. Spatial correlation measurements provide information about the characteristic bias and hence mass of the haloes in which galaxies reside (e.g., Kaiser 1984; Bardeen et al. 1986), and so provide a robust mass estimate that is free of many of the systematics in measuring stellar or black hole masses. The observed clustering of SMGs and QSOs can thus allow us to test whether these populations are found in similar haloes and so may evolve into each other over short timescales. With knowledge of how haloes evolve over cosmic time (e.g., Lacey & Cole 1993; Fakhouri, Ma & Boylan-Kolchin 2010), we can also explore the links to modern elliptical galaxies (e.g., Overzier et al. 2003), as well as the higher-redshift progenitors of SMGs. Clustering measurements can also provide constraints on theoretical studies that explore the nature of SMGs in a cosmological context. Recent models for SMGs as relatively long-lived (> 0.5 Gyr) star formation episodes in the most massive galaxies, driven by the early collapse of the dark matter halo (Xia et al. 2011), or powered by steady accretion of intergalactic gas (Davé et al. 2010), yield strong clustering for bright sources (850 μm fluxes $>$ a few mJy) with correlation lengths $r_0 \gtrsim 10\ h^{-1}$ Mpc. In contrast, models in which SMGs are short-lived bursts in less massive galaxies, with large luminosities produced by a top-heavy initial mass function, predict significantly weaker clustering with $r_0 \sim 6\ h^{-1}$ Mpc (Almeida, Baugh & Lacey 2011).

Attempts to measure the clustering of SMGs from their projected two-dimensional distribution on the sky have for the most part been ambiguous (Scott et al. 2002; Borys et al. 2003; Webb et al. 2003; Weiß et al. 2009; Williams et al. 2011; Lindner et al. 2011). Weiß et al. (2009) used the largest, contiguous extragalactic 870-μm survey (of the Extended *Chandra* Deep Field South; ECDFS), to derive the clustering of $\gtrsim$ 5-mJy SMGs from their projected distribution on the sky. They estimated a correlation length of $13 \pm 6 h^{-1}$ Mpc. Most recently, Williams et al. (2011) analysed a 1100-μm survey of a region of the COSMOS field and placed 1-σ upper limits on the clustering of bright SMGs (with apparent 870-μm fluxes $\gtrsim$ 8–10 mJy) of $\gtrsim$ 6–12 h^{-1} Mpc.

Other work has attempted to improve on angular correlation measurements by including redshift information. Using the spectroscopic redshift survey of 73 SMGs with 870-μm fluxes of $\gtrsim$ 5 mJy spread across seven fields from Chapman et al. (2005), Blain et al. (2004) estimated a clustering amplitude from the numbers of pairs of SMGs within a 1000-km s^{-1} wide velocity window. They derived an effective correlation length of 6.9 ± 2.1 h^{-1} Mpc, suggesting that SMGs are strongly clustered. However their methodology was subsequently criticised by (Adelberger 2005), who suggested that accounting for angular clustering of sources and the redshift selection function significantly increases the uncertainties. Using data from the *Chandra* Deep Field-North, Blake et al. (2006) computed the angular cross-correlation between SMGs and galaxies in slices of spectroscopic and photometric redshift. They obtained a significant SMG-galaxy cross-correlation signal, with hints that SMGs are more strongly clustered than the optically-selected galaxies, although with only marginal ($\sim 2\sigma$) significance. Previous work has therefore pointed toward SMGs being a strongly clustered population, but their precise clustering

amplitude, along with their relationship to QSOs and ellipticals, remains uncertain.

To make improved measurements of the clustering of SMGs, we need either much larger survey areas (see Cooray et al. 2010 for a wide-field clustering measurement for far-IR detected sources) or the inclusion of redshift information (to allow us to reduce the effects of projection on our clustering measurements). To this end, we have reanalysed the Weiß et al. (2009) survey of ECDFS using new spectroscopic and photometric redshift constraints on the counterparts to SMGs (Wardlow et al. 2011) as well as a large catalogue of "normal" (less-active) galaxies in the same field. We employ a new clustering analysis methodology (Myers, White & Ball 2009) to calculate the projected spatial cross-correlation between SMGs and galaxies, to obtain the tightest constraint to date on the clustering amplitude of SMGs.

This paper is organised as follows. In § 2 we introduce the SMG and galaxy samples, and in § 3 we give an overview of the methodology used to measure correlation functions and estimate dark matter (DM) halo masses. In § 4 we present the results, explore the effects of photometric redshift errors, compare with previous measurements, and discuss our results in the context of the physical drivers, lifetimes, and evolutionary paths of SMGs. In § 5 we summarise our conclusions. Throughout this paper we assume a cosmology with $\Omega_m = 0.3$ and $\Omega_\Lambda = 0.7$. For direct comparison with other works, we assume $H_0 = 70$ km s^{-1} Mpc^{-1} (except for comoving distances and DM halo masses, which are explicitly given in terms of $h = H_0/(100$ km s^{-1} Mpc^{-1})). In order to easily compare to estimated halo masses in other recent works on QSO clustering (e.g., Croom et al. 2005; Myers et al. 2006; da Ângela et al. 2008; Ross et al. 2009), we assume a normalisation for the matter power spectrum of $\sigma_8 = 0.84$. All quoted uncertainties are 1σ (68% confidence).

2 SMG AND GALAXY SAMPLES

Our SMG sample comes from the survey of the ECDFS using the Large APEX BOlometer CAmera (Siringo et al. 2009, LABOCA) on the Atacama Pathfinder EXperiment (Güsten et al. 2006, APEX) 12-m telescope (the LABOCA ECDFS Submillimetre Survey, or LESS; Weiß et al. 2009). LESS mapped the full 0.35 deg^2 ECDFS to a 870-μm noise level of $\sim$ 1.2 mJy beam^{-1} and detected 126 SMGs at $> 3.7\sigma$ significance (Weiß et al. 2009, equivalent to a false-detection rate of $\sim$ 4%). Radio and mid-infrared counterparts to LESS SMGs were identified by Biggs et al. (2011) using a maximum-likelihood technique. Spectroscopic and photometric redshifts were obtained for a significant fraction of these counterparts by Wardlow et al. (2011) and we refer the reader to that work for more details. For this study, we restrict our analysis to the 50 SMGs that have secure counterparts at $z = 1$–3 and do not lie close to bright stars (as discussed below). The upper limit of $z = 3$ on the sample is included to maximize overlap in redshift space with the galaxy sample, in order to obtain a significant cross-correlation signal, while the lower bound of $z = 1$ is included to prevent the SMG sample from being biased toward low redshifts. Of the SMGs in the sample, 22 SMGs (44%) have spectroscopic redshifts (Danielson et al., in preparation) and the remainder have photometric redshifts with a typical precision of $\sigma_z/(1+z) \sim 0.1$ (Wardlow et al. 2011). The 870-μm flux distribution for the SMGs having secure counterparts (Biggs et al. 2011) is consistent with that for all LESS SMGs Weiß et al. (2009), indicating that the requirement that SMGs have

secure counterparts does not strongly bias the fluxes of our SMG sample.

For the cross-correlation analysis, we also require a comparison population in the same field. For this we adopt the $\sim 50,000$ galaxies detected in the Spitzer IRAC/MUSYC Public Legacy Survey in the Extended CDF-South (Damen et al. 2011). We use an IRAC selected sample to ensure that each galaxy has photometry in a sufficient number of bands, and over a wide enough wavelength range, to allow robust estimates of photometric redshift. Photo-zs are calculated using template fits to the optical and IRAC photometry in an identical method to that used for the SMGs (see Wardlow et al. 2011). The fits are performed with HYPER-Z (Bolzonella, Miralles & Pelló 2000) and the resulting redshift distribution, compared to that for the SMGs, is shown in Figure 2. The photometric analysis uses chi-squared minimisation, which allows the calculation of confidence intervals for the best-fit redshift. These can be presented as a probability distribution function (PDF) for the redshift, or equivalently, the comoving line-of-sight distance χ (calculated for our assumed cosmology). We define the PDF for each galaxy as $f(\chi)$, where $\int f(\chi)d\chi = 1$. Examples of the PDFs for the galaxies are shown in Figure 3.

Finally, in order to calculate the correlation functions, we first create random catalogues of "galaxies" at random positions within the actual spatial coverage of our survey. Like many fields, the ECDFS contains several bright stars with large haloes, around which few galaxies are detected. Therefore, we use the background map produced by SEXTRACTOR (Bertin & Arnouts 1996) from the combined IRAC image during the source extraction procedure to create a mask. This mask is applied to the random catalogues, the SMGs and the IRAC galaxies, so that the positions of the random galaxies are unbiased with respect to the SMG and IRAC galaxy samples, and thus the mask does not affect the cross-correlation measurement. As discussed in Biggs et al. (2011) and Wardlow et al. (2011), some of the SMG identifications were performed manually by examining the regions around the SMGs. These additional sources are excluded from the clustering analysis so as not to bias the results. The sky positions of the SMGs and galaxies that are outside the masked regions are shown in Figure 1.

3   CORRELATION ANALYSIS

To measure the spatial clustering of SMGs, we can in principle derive the autocorrelation of the SMGs themselves. However, as we have discussed, current SMG samples are too limited in size and available redshift information to make this feasible. Alternatively, we can measure the *cross*-correlation of a population with a sample of other sources (for example, less-active galaxies) which populate the same volume (e.g., Gawiser et al. 2001; Adelberger & Steidel 2005; Blake et al. 2006; Coil et al. 2007; Hickox et al. 2009). The much larger number of galaxies in the ECDFS ($\sim 1000\times$ more than the SMGs in a comparable redshift range) allows far greater statistical accuracy in the measurement of clustering.

To calculate the real-space projected cross-correlation function $w_p(R)$ between SMGs and galaxies we employ a method derived by Myers, White & Ball (2009). This method enables us to take advantage of the full photo-z PDF for each galaxy, by weighting pairs of SMGs and galaxies based on the probability of their overlap in redshift space. This method allows us to calculate the SMG-galaxy cross-correlation using the full sample of $z \approx 50,000$ IRAC galaxies, while the derive the clustering of the galaxies themselves using a smaller sample that is selected to match the overlap
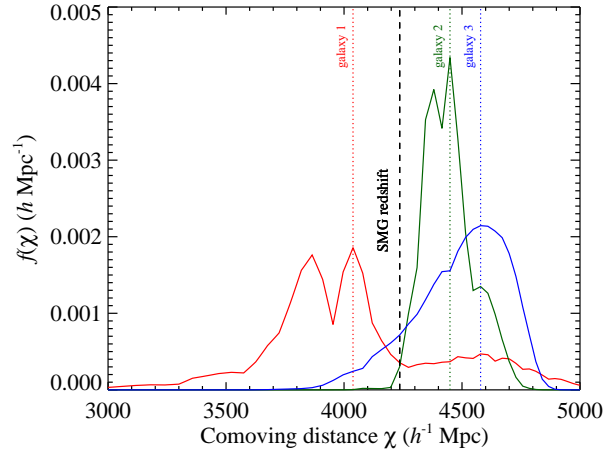

Figure 3. Example probability distribution functions for three IRAC galaxies and an SMG. We mark the "best" (peak) comoving distance for each galaxy. Note that for each galaxy in this example, the line-of-sight distance between the "peak" redshift of the galaxy and the SMG redshift is far too large for them to be physically associated. However, because of the uncertainty in the galaxy redshifts (shown by the PDFs), there is a non-negligible probability that the galaxies lie close to the line-of-sight distance of the SMG.

in the redshift distributions of the galaxies and SMGs. Our clustering analysis is identical in most respects to the QSO-galaxy cross-correlation study presented in Hickox et al. (2011, hereafter H11). Because the method is somewhat involved, we present only the key details here and refer the reader to H11 for a full discussion.

3.1   Cross-correlation method

The two-point correlation function $\xi(r)$ is defined as the probability above Poisson of finding a galaxy in a volume element dV at a physical separation r from another randomly chosen galaxy, such that

$$dP = n[1 + \xi(r)]dV, \tag{1}$$

where n is the mean space density of the galaxies in the sample. The projected correlation function $w_p(R)$ is defined as the integral of $\xi(r)$ along the line of sight,

$$w_p(R) = 2 \int_0^{\pi_{\max}} \xi(R, \pi)d\pi, \tag{2}$$

where R and π are the projected comoving separations between galaxies in the directions perpendicular and parallel, respectively, to the mean line of sight from the observer to the two galaxies. By integrating along the line of sight, we eliminate redshift-space distortions owing to the peculiar motions of galaxies, which distort the line-of-sight distances measured from redshifts. $w_p(R)$ has been used to measure correlations in a number of surveys (e.g., Zehavi et al. 2005; Li et al. 2006; Gilli et al. 2007; Coil et al. 2007, 2008; Wake et al. 2008a; Myers, White & Ball 2009; Hickox et al. 2009; Coil et al. 2009; Gilli et al. 2009; Krumpe, Miyaji & Coil 2010; Donoso et al. 2010; Hickox et al. 2011; Starikova et al. 2011; Allevato et al. 2011).

In the range of separations $0.3 \lesssim r \lesssim 50\ h^{-1}$ Mpc, $\xi(r)$ for galaxies and QSOs is roughly observed to be a power-law,

$$\xi(r) = (r/r_0)^{-\gamma}, \tag{3}$$

with γ typically $\approx$1.8 (e.g., Zehavi et al. 2005; Coil et al. 2008, 2007; Ross et al. 2009). For sufficiently large $\pi_{\max}$ such that we average over all line-of-sight peculiar velocities, $w_p(R)$ can be directly related to $\xi(r)$ (for a power law parameterisation) by

$$w_p(R) = R \left(\frac{r_0}{R}\right)^{\gamma} \frac{\Gamma(1/2)\Gamma[(\gamma - 1)/2]}{\Gamma(\gamma/2)}. \qquad (4)$$

To calculate $w_p(R)$ for the cross-correlation between SMGs and galaxies, we use the method of M09, which accounts for the photometric redshift probability distribution for each galaxy individually. Following M09, the projected cross-correlation function can be calculated using:

$$w_p(R) = N_R N_S \sum_{i,j} c_{i,j} \frac{D_S D_G(R)}{D_S R_G(R)} - \sum_{i,j} c_{i,j} \qquad (5)$$

where

$$c_{i,j} = f_{i,j} / \sum_{i,j} f_{i,j}^2. \qquad (6)$$

Here R is the projected comoving distance from each SMG, for a given angular separation θ and radial comoving distance to the SMG of χ_*, such that $R = \chi_* \theta$. $D_S D_G$ and $D_S R_G$ are the number of SMG–galaxy and SMG–random pairs in each bin of R, and N_S and N_R are the total numbers of SMGs and random galaxies, respectively. $f_{i,j}$ is defined as the average value of the radial PDF $f(\chi)$ for each galaxy i, in a window of size $\Delta \chi$ around the comoving distance to each spectroscopic source j. We use $\Delta \chi = 100 \ h^{-1}$ Mpc to effectively eliminate redshift space distortions, although the results are insensitive to the details of this choice. We refer the reader to M09 and H11 for a detailed derivation and discussion of these equations. In this calculation as well as in the galaxy autocorrelation, we account for the integral constraint as described in H11. This correction increases the observed clustering amplitude by $\approx$15%.

3.2 Galaxy autocorrelation

To estimate DM halo masses for the SMGs, we calculate the relative bias between SMGs and galaxies, from which we derive the absolute bias of the SMGs relative to DM. As discussed below, calculation of absolute bias (and thus halo mass) requires a measurement of the autocorrelation function of the IRAC galaxies. The large size of the galaxy sample enables us to derive the clustering of the galaxies accurately from the angular autocorrelation function $\omega(\theta)$ alone. Although we expect the photometric redshifts for the IRAC galaxies to be reasonably well-constrained (as discussed in § 2), by using the angular correlation function we minimize any uncertainties relating to individual galaxy photo-zs for this part of the analysis. The resulting clustering measured for the galaxies has significantly smaller uncertainties than that for the SMG-galaxy cross-correlation.

We calculate the angular autocorrelation function $\omega(\theta)$ using the Landy & Szalay (1993) estimator:

$$\omega(\theta) = \frac{1}{RR}(DD - 2DR + RR), \qquad (7)$$

where DD, DR, and RR are the number of data-data, data-random, and random-random galaxy pairs, respectively, at a separation θ, where each term is scaled according to the total numbers of SMGs, galaxies, and randoms.

The galaxy autocorrelation varies with redshift, owing to the

evolution of large scale structure, and because the use of a flux-limited sample means we select more luminous galaxies at higher z. This will affect the measurements of relative bias between SMGs and galaxies, since the redshift distribution of the SMGs peaks at higher z than that for the galaxies and so relatively higher-z galaxies dominate the cross-correlation signal. To account for this in our measurement of galaxy autocorrelation, we randomly select galaxies based on the overlap of the PDFs with the SMGs in comoving distance (in the formalism of § 3.1 this is $f_{i,j}$ for each galaxy, averaged all SMGs). We select the galaxies so their distribution in redshift is equivalent to the *weighted* distribution for all galaxies (weighted by $\langle f_{i,j} \rangle$). The redshift distribution of this galaxy sample is shown in Figure 2. We use this smaller galaxy sample to calculate the angular autocorrelation of IRAC galaxies.

3.3 Uncertainties and model fits

We estimate uncertainties on the clustering directly from the data using bootstrap resampling. Following H11, we divide the field into a small number of sub-areas (we choose $N_{\mathrm{sub}} = 8$), and for each bootstrap sample we randomly draw a total of $3N_{\mathrm{sub}}$ sub-areas (with replacement), which has been shown to best approximate the intrinsic uncertainties in the clustering amplitude (Norberg et al. 2009). To account for shot noise owing to the relatively small size of the SMG sample, we take the sets of $3N_{\mathrm{sub}}$ bootstrap sub-areas and randomly draw from them (with replacement) a sample of sources (SMGs or galaxies) equal in size to the parent sample; only pairs including these sources are used in the resulting cross-correlation calculation. We use the bootstrap results to derive the covariance between different bins of R, calculating the covariance matrix using Equation 12 of H11.

We fit the observed $w_p(R)$ with two models: a power law and a simple bias model (described in § 3.4). We compute model parameters by minimising χ^2 (taking into account the covariance matrix as in Equation 13 of H11) and derive 1σ errors in each parameter by the range for which $\Delta \chi^2 = 1$. We use the same formalism for computing fits to the angular correlation functions, where $\omega(\theta) = A\theta^{-\delta}$. We convert A and δ to real-space clustering parameters r_0 and γ following the procedure described in § 4.6 of H11.

3.4 Absolute bias and dark matter halo mass

The masses of the DM haloes in which galaxies and SMGs reside are reflected in their absolute clustering bias b_{abs} relative to the DM distribution. The linear bias b_{abs}^2 is given by the ratio of the autocorrelation function of the galaxies (or SMGs) to that of the DM. We determine b_{abs} following the method outlined in § 4.7 of H11, similar to the approach used previously by a number of studies (e.g., Myers et al. 2006, 2007; Coil et al. 2007, 2008, 2009; Hickox et al. 2009); in what follows we briefly describe this procedure.

We first calculate the two-point autocorrelation of DM as a function of redshift. We use the HALOFIT code of Smith et al. (2003) assuming our standard cosmology, and the slope of the initial fluctuation power spectrum, $\Gamma = \Omega_m h = 0.21$, to derive the DM power spectrum, and thus its projected correlation function $w_p^{\mathrm{DM}}(R)$, averaged over the redshift distribution for which the SMGs and galaxies overlap. We then fit the observed $w_p(R)$ of the SMG-galaxy cross-correlation, on scales 0.3–15 h^{-1} Mpc, with a model comprising a simple linear scaling of $w_p^{\mathrm{DM}}(R)$. The best-fit linear scaling of the DM correlation function corresponds to $b_S b_G$, the product of the linear biases for the SMGs and galaxies, respectively. This simple model produces a goodness-of-fit comparable
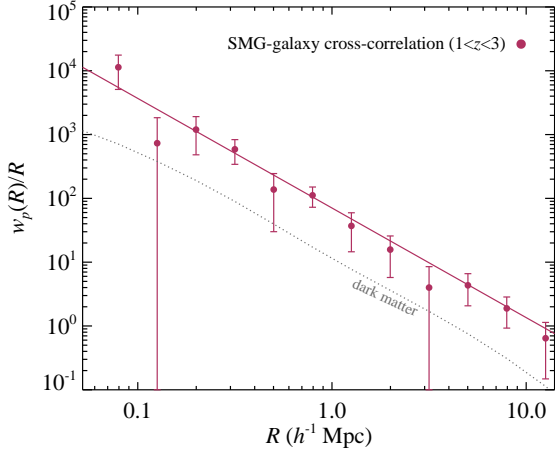
Figure 4. The projected SMG-galaxy cross-correlation function (derived using Equation 5). Uncertainties are estimated from bootstrap resampling. A power-law fit to $w_p(R)$ is shown by the solid line, and the projected correlation function for DM is shown by the dotted line. Fits are performed over the range in separation of $R = 0.3$–15 h^{-1} Mpc. Both the power law model with $\gamma = 1.8$ and a linear scaling of the DM correlation function provide satisfactory fits to the observed $w_p(R)$. Together with the observed galaxy autocorrelation, this measurement yields the clustering amplitude and DM halo mass for the SMGs, as described in § 4.

Figure 5. The angular autocorrelation function of IRAC galaxies, selected to match the overlap of the SMGs and galaxies in redshift space. Uncertainties are estimated from bootstrap resampling. The angular correlation function for DM, evaluated for the redshift distributions of the galaxies, is shown by the dotted gray line. The power law fit was performed on scales $0.3'$–$10'$ and is shown as the solid line. Both the power law model with $\delta = 0.8$ and a linear scaling of the DM correlation function provide satisfactory fits to the observed $\omega(\theta)$. The observed amplitude of the galaxy autocorrelation yields the absolute bias of the galaxies, which we use to obtain the absolute bias and DM halo mass of the SMGs.

to that of the power-law model in which the slope γ is allowed to float.

To determine b_S we therefore need to estimate b_G. We obtain b_G for the galaxies from their angular autocorrelation in a similar manner to that applied to the SMG–galaxy cross-correlation. Again we calculate the autocorrelation for the DM $\omega_{DM}(\theta)$, by integrating the power spectrum from HALOFIT using Equation (A6) of Myers et al. (2007). We fit the observed $\omega(\theta)$ with a linear scaling of $\omega_{DM}(\theta)$ on scales $0.3'$–$10'$ (corresponding to 0.3–10 h^{-1} Mpc at $z = 2$). This linear scaling corresponds to b_G^2 and thus (combined with the cross-correlation measurement) yields the SMG bias b_S. Finally, we convert b_G and b_S to $M_{\rm halo}$ using the prescription of Sheth, Mo & Tormen (2001), as described in H11. This characteristic $M_{\rm halo}$ corresponds to the top-hat virial mass (see e.g., Peebles 1993, and references therein), in the simplified case in which all objects in a given sample reside in haloes of the same mass. This assumption is justified by the fact (as discussed below in § 4.4) that SMGs have a very small number density compared to the population of similarly-clustered DM haloes, such that it is reasonable that SMGs may occupy haloes in a relatively narrow range in mass. We note that this method differs from some prescriptions in the literature which assume that sources occupy all haloes above some minimum mass; this is particularly relevant for populations with high number densities that could exceed the numbers of available DM haloes over a limited mass range. Given the halo mass function at $z \sim 2$ (e.g., Tinker et al. 2008) the derived minimum mass is typically a factor of ~ 2 lower, for the same clustering amplitude, than the "average" mass quoted here.

4   RESULTS AND DISCUSSION

The projected cross-correlation function of the SMG sample with the IRAC galaxies is shown in Figure 4. We plot the best-fit power-
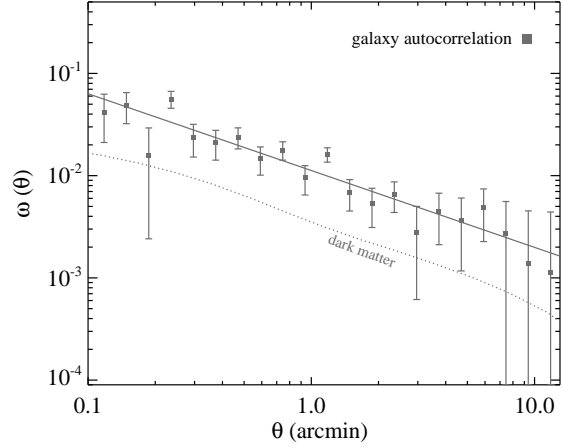
law model, and show the correlation function of the DM calculated as in § 3.4, which we fit to the data through a linear scaling. The power-law and linear bias fit parameters are presented in in Table 1. For SMGs the observed real-space projected cross-correlation is well-detected on all scales from 0.1–15 h^{-1} Mpc, and the power-law fits return $\gamma \sim 1.8$, similar to many previous correlation function measurements for galaxies (e.g., Zehavi et al. 2005; Coil et al. 2008) and QSOs (e.g., Coil et al. 2007; Ross et al. 2009). The best-fit parameters for the SMG-galaxy cross-correlation are $r_{0,SG} = 5.3 \pm 0.8$ h^{-1} Mpc, $\gamma = 1.7 \pm 0.2$. If we fix the value of γ to 1.8, we obtain $r_{0,SG} = 5.1 \pm 0.6$ h^{-1} Mpc, corresponding to a clustering signal that is significant at the $> 4\sigma$ level, the most significant measurement of SMG clustering to date. From the fit of the DM model, we obtain $b_S b_G = 5.83 \pm 1.36$.

We next compute the autocorrelation of IRAC galaxies for the sample described in § 3.2. The observed $\omega(\theta)$ is shown in Fig. 5, along with the corresponding power-law fit and scaled correlation function for DM, calculated as discussed in §3.4. Fit parameters are given in Table 1. The power-law model fits well on the chosen scales of $0.3'$–$10'$. The best-fit power law parameters are $r_{0,GG} = 3.3 \pm 0.3$ and $\gamma = 1.8 \pm 0.2$, and the best-fit scaled DM model yields $b_G^2 = 2.99 \pm 0.40$ or $b_G = 1.73 \pm 0.12$.

This accurate value for b_G yields $b_S = 3.37 \pm 0.82$ for the SMGs. Converting this to DM halo mass using the prescription of Sheth, Mo & Tormen (2001) as described in §3.4, we arrive at $\log\left(M_{\rm halo}[h^{-1} M_\odot]\right) = 12.8^{+0.3}_{-0.5}$. The corresponding halo mass for the galaxies is $\log\left(M_{\rm halo}[h^{-1} M_\odot]\right) = 11.5 \pm 0.2$.

For comparison with other studies that attempted to directly measure the autocorrelation function of SMG, it is useful to present the SMG clustering in terms of effective power-law parameters for their autocorrelation. Assuming linear bias, the SMG autocorrelation can be inferred from the cross-correlation by $\xi_{SS} = \xi_{SG}^2/\xi_{GG}$ (e.g., Coil et al. 2009). Adopting a fixed $\gamma = 1.8$ for the SMG-

Table 1. Correlation results

| Subset | $N_{\rm src}$[a] | $\langle z \rangle$[b] | Power law fit[c] | | | Bias model fit[d] | | | Halo mass[e] |
			r_0 (h^{-1} Mpc)	γ	χ^2_ν	$b_S b_G$ (b_G^2)	b_S (b_G)	χ^2_ν	(log h^{-1} $M_\odot$)
SMGs	50	2.02	$7.7^{+1.8}_{-2.3}$	1.8 ± 0.2	0.8	5.83 ± 1.36	3.37 ± 0.82	0.7	$12.8^{+0.3}_{-0.5}$
galaxies	11,241	2.13	3.3 ± 0.3	1.8 ± 0.2	1.8	2.99 ± 0.40	1.73 ± 0.12	1.8	11.5 ± 0.2

[a] Number of objects in the SMG sample and in the galaxy sample used for the galaxy autocorrelation.

[b] Median redshift for the SMG sample and for the galaxy sample used for the galaxy autocorrelation.

[c] Power law model parameters are for the autocorrelation of SMGs (derived from SMG-galaxy projected spatial cross-correlation, along with the galaxy angular autocorrelation) and galaxies (derived from their angular autocorrelation).

[d] Parameters derived from the observed linear fit of the DM model to the observed correlation function, in order to obtain the the absolute bias for the SMGs and galaxies (denoted b_S and b_G, respectively). The linear scaling from the fit corresponds to $b_S b_G$ for the SMG-galaxy cross-correlation, and b_G^2 for the galaxy autocorrelation, which in turn yield b_G and b_S.

[e] DM halo mass derived from the absolute bias, using the method described in § 3.4.

galaxy cross-correlation, we thus obtain $r_{0,SS} = 7.7^{+1.8}_{-2.3}$ h^{-1} Mpc for the autocorrelation of the SMGs.

4.1 Effects of SMG photo-z errors

One uncertainty in our estimate of $w_p(R)$ for the SMG-galaxy cross-correlation is due to the lack of accurate (that is, spectroscopic) redshifts for roughly half of the SMG population. As described in § 3, in calculating $w_p(R)$ for the cross-correlation, we simply assume that the SMGs lie exactly at the best redshifts from the photo-z analysis of Wardlow et al. (2011). Any uncertainties in the SMGs photo-zs could therefore affect the resulting clustering measurement. (Note that photo-z uncertainties in the galaxies are accounted for implicitly in the correlation analysis, as we utilize the full galaxy photo-z PDFs.) To examine the effects of SMG photo-z errors, we follow the procedure outlined in § 6.3 of H11. We take advantage of the 44% of SMGs that do have spectroscopic redshifts, and determine how errors in those redshifts affect the observed correlation amplitude.

Specifically, we shift the redshifts of the spectroscopic SMGs by offsets $\Delta z/(1+z)$ selected from a Gaussian random distribution with dispersion $\sigma_z/(1+z)$. To ensure that this step does not artificially smear out the redshift distribution beyond the range probed by the galaxies, we require that the random redshifts lie between $1 < z < 3$; any random redshift that lies outside this range is discarded and a new redshift is selected from the random distribution. Using these new redshifts we recalculate $w_p(R)$, using the full formalism described in § 3. We perform the calculation 10 times for each of several values of $\sigma_z/(1 + z)$ from 0.05 up to 0.3 (corresponding to the range of photo-z uncertainties). For each trial we obtain the relative bias by calculating the mean ratio of $w_p(R)$, on scales 1–10 h^{-1} Mpc, relative to the $w_p(R)$ for the best estimates of redshift. We then average the ten trials at each σ_z, and find that at most the photo-z errors cause the clustering amplitude to decrease by $\sim 10\%$. The precise magnitude of this effect is unclear given the range of uncertainties in the SMG photo-z estimates, but it is is significantly smaller than the statistical uncertainties. We therefore neglect this effect in our final error estimates.

4.2 Comparison with previous results

Here we compare our results to other measurements of SMG clustering in the literature. The observed clustering may depend on the flux limit of the submm sample, as discussed by Williams et al. (2011); measurements of r_0 that use SMG samples with similar

submm flux limits are shown in Figure 6a. Our measurement is significantly more accurate than previous measurements, owing to the inclusion of redshift information and the improved statistics in the cross-correlation. The uncertainties are comparable to those quoted by Blain et al. (2004) who estimated r_0 using counts of close pairs in redshift space from spectroscopic surveys. However, these authors did not account for significant additional sources of error, as discussed by Adelberger (2005). Uncertainties in the redshift selection function for spectroscopic objects, along with the presence of redshift spikes and angular clustering of sources, can strongly impact the number of expected pair counts for an unclustered distribution, and therefore significantly affect the results for the clustering amplitude (Adelberger 2005). In Figure 6a the large error bars for the Blain et al. (2004) point represent the increase in the uncertainty by 60% due to angular clustering of sources and redshift spikes (as estimated by Adelberger 2005), but does not include the additional uncertainty on the redshift selection function. Nonetheless, our measurement of r_0 is consistent with most previous angular clustering estimates as well as the Blain et al. (2004) result, and represents a significant improvement in precision.

As discussed in § 3.4, we convert the observed clustering amplitude to $M_{\rm halo}$ by assuming that SMGs obey simple linear bias relative to the dark matter and reside in haloes of similar mass. Motivated by the presence of a large overdensity of SMGs and powerful star-forming galaxies in one redshift survey field, Chapman et al. (2009) proposed that SMGs obey "complex bias" that depends on large-scale environment and merger history, and that they may reside in somewhat smaller haloes than would be inferred from a linear bias model. Future studies using significantly larger SMG samples may be able to confirm the existence of more complex clustering, but for the present analysis we adopt the simplest scenario and derive $M_{\rm halo}$ assuming linear bias.

The characteristic halo mass we measure for SMGs is similar to that measured for bright far-IR sources (with fluxes $>$ 30 mJy at 250 μm) detected by the *Herschel Space Observatory* using an angular clustering analysis (Cooray et al. 2010). While it remains uncertain to what extent bright 250 μm sources and 850 μm-selected SMGs represent a common population, both samples comprise the luminous end of the star-forming galaxy population detected at those wavelengths and so may represent physically similar systems. In contrast, our observed SMG clustering is significantly stronger than that reported by Amblard et al. (2011) for "submillimetre galaxies" based on a power-spectrum analysis of *Herschel* 350 μm maps, which yields a minimum $M_{\rm halo}$ of $\sim 3 \times 10^{11}$ $M_\odot$. The differences in clustering amplitude compared to SMGs result from the fact that the power spectrum analysis includes unresolved

faint sources corresponding to far fainter far-IR luminosities, characteristic of typical $z \sim 2$ star-forming galaxies rather than the powerful, luminous starbursts that are conventionally referred to as SMGs in the literature.

4.3 Progenitors and descendants of SMGs

Our improved clustering measurement allows us to place SMGs in the context of the cosmological history of star formation and growth of DM structures. Because the clustering amplitude of dark matter haloes and their evolution with redshift are directly predicted by simulations and analytic theory, we can use the observed clustering to connect the SMG populations to their descendants and progenitors, estimate lifetimes, and constrain starburst triggering mechanisms.

We first compare the clustering amplitude of SMGs with other galaxy populations over a range of redshifts[1]. Figure 6b shows the approximate ranges of measurements of r_0 for a variety of galaxy and AGN populations. We also show the evolution of r_0 with redshift for DM haloes of different masses, determined by fitting a power law with $\gamma = 1.8$ to the DM correlation function output by HALOFIT. Finally, we show the observed r_0 for the current SMG sample, along with the expected evolution in r_0 for haloes that have the observed $M_{\rm halo}$ for SMGs at $z = 2$, calculated using the median growth rate of haloes as a function of $M_{\rm halo}$ and z (Fakhouri, Ma & Boylan-Kolchin 2010)[2].

Figure 6b shows that while the DM halo mass for the SMGs will increase with time from $z \sim 2$ to $z = 0$, the observed r_0 stays essentially constant, meaning that the progenitors and descendants of SMGs will be populations with similar clustering amplitudes. Our measurement of r_0 shows that the clustering of SMGs is consistent with optically-selected QSOs (e.g., Croom et al. 2005; Myers et al. 2006; da Ângela et al. 2008; Ross et al. 2009). SMGs are more strongly clustered than the typical star-forming galaxy populations at all redshifts (e.g. Adelberger et al. 2005; Gilli et al. 2007; Hickox et al. 2009; Zehavi et al. 2011), and are clustered similarly or weaker than massive, passive systems (e.g., Quadri et al. 2007, 2008; Wake et al. 2008b; Blanc et al. 2008; Kim et al. 2011; Zehavi et al. 2011). The clustering results indicate that SMGs will likely evolve into the most massive, luminous early type galaxies at low redshift. We note that the descendants of typical SMGs are not likely to reside in massive clusters at $z = 0$, but into moderate- to high-mass groups of $\sim$ a few $\times 10^{13}$ h^{-1} $M_\odot$. Although *some* SMGs could evolve into massive cluster galaxies, the observed clustering suggests that most will end up in less massive systems.

A schematic picture of the evolution of SMGs is shown in Figure 7, which shows evolution in the mass of haloes with redshift as traced by their median growth rate (Fakhouri, Ma & Boylan-Kolchin 2010). The typical progenitors of SMGs would have $M_{\rm halo} \sim 10^{12}$ h^{-1} $M_\odot$ at $z \sim 5$, which corresponds to the host haloes of bright LBGs at those redshifts (e.g., Hamana et al. 2004; Lee et al. 2006). At low redshift, the SMG descendants will have $M_{\rm halo} = (0.6–5) \times 10^{13}$ h^{-1} $M_\odot$. Halo occupation distribution fits to galaxy clustering suggest that these haloes host galaxies with luminosities $L \sim 2–3L^*$ (Zehavi et al.

---

[1] Myers et al. (2006) and Ross et al. (2009) determine r_0 from QSOs assuming a power law correlation function with $\gamma = 2$. To estimate r_0 for $\gamma = 1.8$, we multiply the quoted values by 0.8, appropriate for fits over the range $1 \lesssim R \lesssim 100$ h^{-1} Mpc.
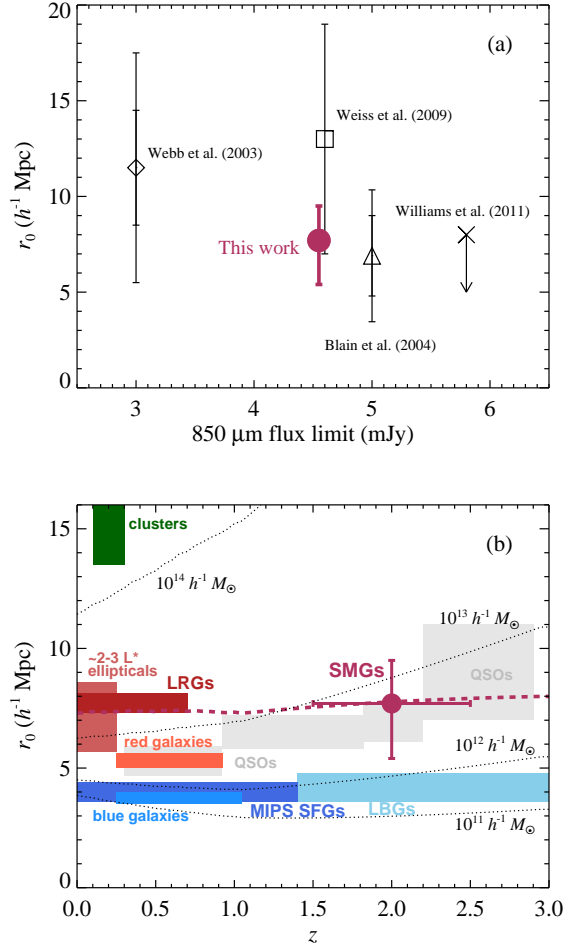

Figure 6. (*a*) Our new measurement of the autocorrelation length r_0 for SMGs, compared to previous results using samples with similar $\sim$850 μm flux limits. The two sets of error bars on the Webb et al. (2003) measurement indicate statistical (± 3 h^{-1} Mpc) and systematic (± 3 h^{-1} Mpc) uncertainties separately. On the Blain et al. (2004) measurement, the smaller errors represent the uncertainties quoted by the authors, while the larger errors account for angular clustering and redshift spikes as estimated by Adelberger (2005). Our results are consistent with previous measurements and represent a significant improvement in precision. (*b*) Our measurement of the autocorrelation length r_0 of SMGs, compared to the approximate r_0 (with associated measurement uncertainties) for a variety of galaxy and AGN populations: optically-selected SDSS QSOs at $0 < z < 3$ (Myers et al. 2006; Ross et al. 2009), Lyman-break galaxies (LBGs) at $1.5 \lesssim z \lesssim 3.5$ (Adelberger et al. 2005), MIPS 24 μm-selected star-forming galaxies at $0 < z < 1.4$ (Gilli et al. 2007), typical red and blue galaxies at $0.25 \lesssim z \lesssim 1$ from the AGES (Hickox et al. 2009) and DEEP2 (Coil et al. 2008) spectroscopic surveys, luminous red galaxies (LRGs) at $0 < z < 0.7$ (Wake et al. 2008b), and optically-selected galaxy clusters at $0.1 < z < 0.3$ (Estrada, Sefusatti & Frieman 2009). In addition, we show the full range of r_0 for low-redshift galaxies with r-band luminosities in the range 1.5 to 3.5 L^*, derived from the luminosity dependence of clustering presented by Zehavi et al. (2011); these luminous galaxies are primarily ellipticals, as discussed in § 4.3. Dotted lines show r_0 versus redshift for DM haloes of different masses. The thick solid line shows the expected evolution in r_0, accounting for the increase in mass of the halo, for a halo with mass corresponding to the best-fit estimate for SMGs at $z = 2$. The results indicate that SMGs are clustered similarly to QSOs at $z \sim 2$ and can be expected to evolve into luminous elliptical galaxies in the local Universe.
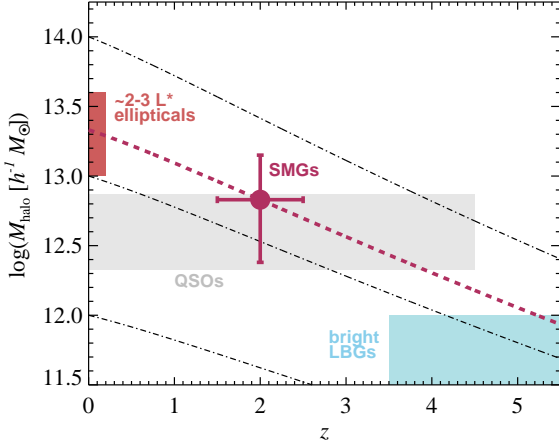
Figure 7. Broad schematic for the evolution of halo mass versus redshift for SMGs, showing the approximate halo masses corresponding to likely progenitors and descendants of SMGs. Lines indicate the median growth rates of haloes with redshift (Fakhouri, Ma & Boylan-Kolchin 2010). SMG host haloes are similar to those those of QSOs at $z \sim 2$, and correspond to bright LBGs at $z \sim 5$ (Hamana et al. 2004; Lee et al. 2006) and ~ 2–$3L^*$ ellipticals at $z = 0$ (Zehavi et al. 2011; Stott et al. 2011).

2011), a population dominated by ellipticals with predominantly slow-rotating kinematics (e.g., Tempel et al. 2011; Cappellari et al. 2011). Assuming typical mass-to-light ratios for massive galaxies (e.g., Baldry, Glazebrook & Driver 2008), these luminosities correspond to stellar masses $\sim (1.5$–$2.5) \times 10^{11} M_\odot$, in close agreement with direct measurements of the relationship between halo mass and central galaxy stellar mass for X-ray selected groups and clusters, for which $\log M_\star \approx 0.27 \log M_{\mathrm{halo}} + 7.6$ (Stott et al. 2011).

4.4 SMG lifetime and star formation history

We next estimate the SMG lifetime, making the simple assumption that every dark matter halo of similar mass passes through an SMG phase[3], so that

$$t_{\mathrm{SMG}} = \Delta t \frac{n_{\mathrm{SMG}}}{n_{\mathrm{halo}}}, \qquad (8)$$

where Δt is the time interval over the redshift range covered by the SMG sample, and n_{SMG} and n_{halo} are the space densities of SMGs and DM haloes, respectively.

Using the halo mass function of Tinker et al. (2008), the space density of haloes with $\log \left(M_{\mathrm{halo}}[h^{-1} M_\odot] \right) = 12.8^{+0.3}_{-0.5}$ is $dn_{\mathrm{halo}}/d \ln M = (2.1^{+7.3}_{-1.5}) \times 10^{-4}$ Mpc^{-3}. We adopt a space density of SMGs at $z \sim 2$ of $\sim 2 \times 10^{-5}$ Mpc^{-3}, corresponding to results from previous surveys (e.g., Chapman et al. 2005; Coppin et al. 2006; Schael et al. in preparation). This density is $\sim 50\%$ higher than that observed in the LESS field (Wardlow et al.

---

[2] Note that here we use the median growth rate of haloes, which for haloes of $\sim 10^{13} \, h^{-1} \, M_\odot$ is $\approx 35\%$ lower than the *mean* growth rate, owing to the long high-mass tail in the halo mass distribution.
[3] If the average halo experiences more or fewer SMG phases in the given time interval, the lifetime of each episode will be correspondingly shorter or longer, respectively.

2011), which has been shown to contain a somewhat smaller density of SMGs compared to other surveys (Weiß et al. 2009).

The ratio of these space densities yields a duty cycle (the fraction of haloes that host an SMG at any given time) of $\sim 10\%$. We assume the SMGs occupy the redshift range $1.5 < z < 2.5$, which includes roughly half of the SMGs in the Wardlow et al. (2011) sample and corresponds to $\Delta t = 1.6$ Gyr. We thus obtain a lifetime for SMGs of $t_{\mathrm{SMG}} = 110^{+280}_{-80}$ Myr. Clearly, even our improved measurement of SMG clustering yields only a weak constraint on the lifetime, but this is consistent with lifetimes estimated from gas consumption times and star-formation timescales (e.g., Greve et al. 2005; Tacconi et al. 2006; Hainline et al. 2011) and theoretical models of SMG fueling through mergers (e.g., Mihos & Hernquist 1994; Springel, Di Matteo & Hernquist 2005; Narayanan et al. 2010).

Constraints on SMG descendants from clustering can also yield insights into their their formation histories. Measurements of the stellar plus molecular gas masses of SMGs from SED fitting and dynamical studies are in the range $\sim (1$–$5) \times 10^{11} \, M_\odot$ (Swinbank et al. 2006; Wardlow et al. 2011; Hainline et al. 2011; Ivison et al. 2011; Michałowski et al. 2011). While these estimates can be uncertain by factors of a few, they are in a similar range to the stellar masses of SMG descendants as indicated by their clustering, as discussed above. This correspondence suggests that if a significant fraction of the molecular gas is converted to stars during the SMG phase, then these galaxies will subsequently experience relatively little growth in mass from $z \sim 2$ to the present. This in turn puts limits on the star formation history. Star-forming galaxies at $z \sim 2$ typically exhibit specific star formation rates of $\dot{M}_\star / M_\star \sim 2 \, \mathrm{Gyr}^{-1}$ (Elbaz et al. 2011), at which the SMGs would only need to form stars for 500 Myr in order to double in mass. We may therefore conclude, from the clustering and stellar masses alone, that the SMGs evolve from star-forming to passive states relatively quickly (within a Gyr or so) after the starburst phase, and that the descendants spend most of their remaining time as relatively passive systems. This scenario is consistent with measurements of the stellar populations in ~ 2–$3 \, L^*$ ellipticals, which have typical ages of ~ 10 Gyr and show little evidence for younger components (e.g., Nelan et al. 2005; Allanson et al. 2009), implying that the vast majority of stars were formed above $z \sim 2$ with little additional star formation at lower redshifts.

The halo masses of SMGs may also provide insight into the processes that prevent their descendants from forming new stars. Star formation can be shut off rapidly at the end of the SMG phase, either by exhaustion of the gas supply, or by energy input from a QSO (e.g., Di Matteo, Springel & Hernquist 2005; Springel, Di Matteo & Hernquist 2005). Powerful winds are observed in luminous AGN (e.g., Feruglio et al. 2010; Fischer et al. 2010; Sturm et al. 2011; Greene et al. 2011) and have also been seen in some SMGs (e.g., Alexander et al. 2010, Harrison et al. in preparation), although for the SMGs is unclear whether the winds are driven by the starburst or AGN. Even if the formation of stars is rapidly quenched, over longer timescales the galaxy would be expected to accrete further gas from the surrounding halo, resulting in significant additional star formation (e.g., Bower et al. 2006; Croton et al. 2006). Recent work suggests that energy from accreting supermassive black holes, primarily in the form of radio-bright relativistic jets, can couple to the hot gas in the surrounding halo, producing a feedback cycle that prevents rapid cooling (e.g., Rafferty, McNamara & Nulsen 2008). This mechanical black hole feedback is an key ingredient of successful models for the passive galaxy population (e.g., Croton et al. 2006; Bower et al. 2006;
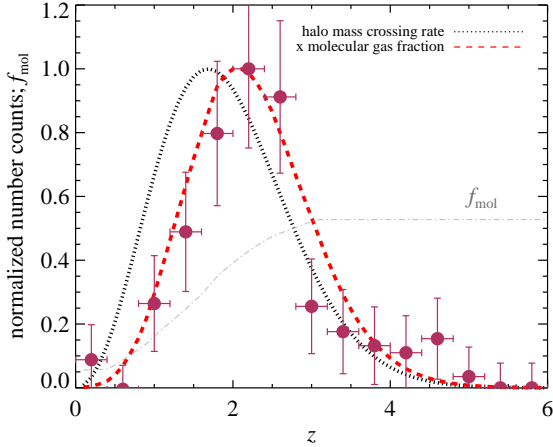
Figure 8. Redshift distribution of LESS SMGs (Wardlow et al. 2011), compared to the simple models for SMG triggering based on the rate at which haloes cross a threshold mass $M_{\mathrm{thresh}} = 6 \times 10^{12} \ h^{-1} \ M_\odot$ (see § 4.5). The uncertainties in the number counts are an approximation of Poisson counting statistics (Gehrels 1986). The black dotted line shows the (arbitrarily normalized) number of haloes crossing this threshold in each redshift interval (Equation 9) while the dashed red line shows this distribution multiplied by the evolution in the molecular gas fraction (Equation 10), where f_{mol} is taken from the model predictions of Lagos et al. (2011) and is shown by the gray dot-dashed line. The remarkable agreement between the second model and the observed number counts suggests that the evolution of the SMG population can be described simply in terms of two quantities: the growth of DM structures and the variation with redshift of the molecular gas fraction in galaxies.

Bower, McCarthy & Benson 2008; Somerville et al. 2008). Interestingly, the clustering of radio galaxies at $z \lesssim 0.8$ indicates that they reside in haloes of mass $\gtrsim 10^{13} \ h^{-1} \ M_\odot$ (e.g., Wake et al. 2008a; Hickox et al. 2009; Mandelbaum et al. 2009; Donoso et al. 2010; Fine et al. 2011), precisely the environments that will host the descendants of SMGs. Thus the strong observed clustering for SMGs can relate them directly to the radio-bright active galactic nucleus population that may regulate their subsequent star formation.

4.5 Evolutionary links with QSOs and the SMG redshift distribution

Finally, the observed clustering of SMGs provides insights into the processes that trigger and (possibly) shut off their rapid star formation activity. As discussed in § 1, powerful local starbursts (i.e. ULIRGs) are predominantly associated with major mergers and appear to be associated with the fueling of luminous QSOs as part of an evolutionary sequence (e.g., Sanders et al. 1988). However it is unclear if a similar connection exists between SMGs and high-z QSOs. One robust prediction of any evolutionary picture is that SMGs and QSOs *must* display comparable large-scale clustering, since the evolutionary timescales are significantly smaller than those for the growth of DM haloes. At all redshifts, QSOs are found in haloes of similar mass $\sim$ a few $\times 10^{12} \ h^{-1} \ M_\odot$ (e.g., Croom et al. 2005; Myers et al. 2006; da Ângela et al. 2008; Ross et al. 2009; Figure 6). The characteristic M_{halo} provides a strong constraint on models of QSO fueling by the major mergers of gas-rich galaxies (e.g., Kauffmann & Haehnelt 2000;

Springel, Di Matteo & Hernquist 2005; Hopkins et al. 2006), secular instabilities (e.g., Mo, Mao & White 1998; Bower et al. 2006; Genzel et al. 2008) or accretion of recycled cold gas from evolved stars (Ciotti & Ostriker 2007; Ciotti, Ostriker & Proga 2010), and is similar to the mass at which galaxy populations transition from star-forming to passive (e.g., Coil et al. 2008; Brown et al. 2008; Conroy & Wechsler 2009; Tinker & Wetzel 2010). The observed clustering of SMGs at $z \sim 2$ from the present work is consistent with that for QSOs, as well as highly active obscured objects including powerful obscured AGN (H11; Allevato et al. 2011) and dust-obscured galaxies (Brodwin et al. 2008). Thus these may indeed represent different phases in the same evolutionary sequence, and energy input from the QSO may be responsible for the rapid quenching of star formation at the end of the SMG phase (e.g., Di Matteo, Springel & Hernquist 2005; Springel, Di Matteo & Hernquist 2005) as discussed in § 4.4.

A connection with QSOs may imply that triggering of SMGs is also related (at least indirectly) to the mass of the parent DM halo. In this case, the evolution of large-scale structure may broadly explain why the SMG population peaks at $z \sim 2.5$ and falls at higher and lower redshifts. In the simplest possible such scenario, SMG activity is triggered when the halo reaches a certain mass $M_{\mathrm{halo}} = M_{\mathrm{thresh}}$ (see Figure 16 of Hickox et al. 2009 for a schematic illustration of this picture). In a given volume, the number of haloes crossing this mass threshold as a function of redshift is:

$$\frac{\mathrm{d}N_{\mathrm{thresh}}}{\mathrm{d}z} \propto n_{\mathrm{halo}}(M_{\mathrm{thresh}}, z)\dot{M}_{\mathrm{halo}}(M_{\mathrm{thresh}}, z)t_{\mathrm{SMG}}\frac{\mathrm{d}V}{\mathrm{d}z}, \quad (9)$$

where n_{halo} and $\dot{M}_{\mathrm{halo}}$ are the number density (e.g., Tinker et al. 2008) and typical growth rate (Fakhouri, Ma & Boylan-Kolchin 2010), respectively, of haloes of mass M_{thresh} at redshift z, t_{SMG} is the SMG lifetime, and $\mathrm{d}V/\mathrm{d}z$ is the differential comoving volume over the survey area. If an SMG is triggered every time a halo reaches M_{thresh}, then the observed number density of SMGs will be proportional to $\mathrm{d}N_{\mathrm{thresh}}/\mathrm{d}z$. However, the huge star formation rates of SMGs require a large reservoir of molecular gas (e.g., Greve et al. 2005; Tacconi et al. 2006, 2008), and the molecular gas fraction increases strongly with redshift (e.g., Tacconi et al. 2010; Geach et al. 2011; Lagos et al. 2011). This evolution may explain why the most powerful starbursts at low redshift (ULIRGs) have lower typical SFRs than $z \sim 2$ SMGs (e.g., Le Floc'h et al. 2005; Rodighiero et al. 2010). Therefore it may be reasonable to assume that the number counts of SMGs also depend on f_{mol}, with the simplest possible prescription being:

$$\frac{\mathrm{d}N_{\mathrm{SMG}}}{\mathrm{d}z} \propto \frac{\mathrm{d}N_{\mathrm{thresh}}}{\mathrm{d}z}f_{\mathrm{mol}}(z). \quad (10)$$

In Figure 8 we show the observed redshift distribution of LESS SMGs (Wardlow et al. 2011), compared to the distributions predicted by Equations (9) and (10), assuming $M_{\mathrm{thresh}} = 6 \times 10^{12} \ h^{-1} \ M_\odot$. For simplicity, the evolution in f_{mol} is taken from predictions of the GALFORM model of Lagos et al. (2011), which agrees broadly with observations (see Figure 2 of Geach et al. 2011) and so provides a simple parameterisation of the current empirical limits on the molecular gas fraction in galaxies. It is clear from Figure 8 that there is remarkable correspondence between our extremely simple prescription and the observed redshifts of SMGs. Of course this "model" does not account for a wide range of possible complications and the normalisations of the distributions are arbitrary. However, this exercise clearly demonstrates that if SMGs, like QSOs, are found in haloes of a characteristic mass, then their observed redshift distribution may be explained simply by two ef-

fects: the cosmological growth of structure combined with the evolution of the molecular gas fraction. Thus SMGs likely represent a short-lived but universal phase in massive galaxy evolution, associated with the transition between cold gas-rich, star-forming galaxies and passively evolving systems.

5 CONCLUSIONS

In this paper we measure the cross-correlation between SMGs and galaxies in the LESS survey of ECDFS, and observe significant clustering at the $> 4\sigma$ level. We obtain an autocorrelation length for the SMGs of $r_0 = 7.7^{+1.8}_{-2.3}\ h^{-1}$ Mpc, assuming $\gamma = 1.8$. This clustering amplitude corresponds to a characteristic DM halo mass of $\log\left(M_{\rm halo}[h^{-1}\ M_\odot]\right) = 12.8^{+0.3}_{-0.5}$. Using this estimate of $M_{\rm halo}$ and the space density of SMGs, we obtain a typical SMG lifetime of $t_{\rm SMG} = 110^{+280}_{-80}$ Myr.

The observed clustering indicates that the low-redshift descendants of typical SMGs are massive (~ 2–$3\ L^*$) elliptical galaxies at the centers of moderate- to high-mass groups. This prediction is consistent with previous suggestions based on the dynamical (Swinbank et al. 2006) and stellar masses (e.g., Hainline et al. 2011) of SMGs, and is also consistent with observations of local massive ellipticals, which indicate that they formed the bulk of their stars at $z > 2$ and have been largely passive since. The clustering of SMGs is very similar to that observed for QSOs at the same redshifts, consistent with evolutionary scenarios in which SMGs and QSOs are triggered by a common mechanism. Assuming that SMGs, like QSOs, are transient phenomena that are observed in haloes of similar mass at all redshifts, the redshift distribution of SMGs can be explained remarkably well by the combination of the cosmological growth of structure and the evolution of the molecular gas fraction in galaxies.

This accurate clustering measurement thus provides a valuable observational constraint on the role of SMGs in the cosmic evolution of galaxies and large-scale structures. We conclude that SMGs likely represent a short-lived but universal phase in massive galaxy evolution that is associated with the rapid growth of black holes as luminous QSOs, and corresponds to the transition between cold gas-rich, star-forming galaxies and passively evolving systems.

REFERENCES

Adelberger K. L., 2005, ApJ, 621, 574
Adelberger K. L., Steidel C. C., 2005, ApJ, 630, 50

Adelberger K. L., Steidel C. C., Pettini M., Shapley A. E., Reddy N. A., Erb D. K., 2005, ApJ, 619, 697
Alexander D. M., Bauer F. E., Chapman S. C., Smail I., Blain A. W., Brandt W. N., Ivison R. J., 2005, ApJ, 632, 736
Alexander D. M. et al., 2008, AJ, 135, 1968
Alexander D. M., Swinbank A. M., Smail I., McDermid R., Nesvadba N. P. H., 2010, MNRAS, 402, 2211
Allanson S. P., Hudson M. J., Smith R. J., Lucey J. R., 2009, ApJ, 702, 1275
Allevato V. et al., 2011, ApJ, 736, 99
Almeida C., Baugh C. M., Lacey C. G., 2011, MNRAS, 417, 2057
Amblard A. et al., 2011, Nature, 470, 510
Assef R. J. et al., 2011, ApJ, 728, 56
Baldry I. K., Glazebrook K., Driver S. P., 2008, MNRAS, 388, 945
Bardeen J. M., Bond J. R., Kaiser N., Szalay A. S., 1986, ApJ, 304, 15
Barger A. J., Cowie L. L., Sanders D. B., Fulton E., Taniguchi Y., Sato Y., Kawara K., Okuda H., 1998, Nature, 394, 248
Bennert V. N., Treu T., Woo J.-H., Malkan M. A., Le Bris A., Auger M. W., Gallagher S., Blandford R. D., 2010, ApJ, 708, 1507
Bertin E., Arnouts S., 1996, A&AS, 117, 393
Biggs A. D. et al., 2011, MNRAS, 413, 2314
Blain A. W., Chapman S. C., Smail I., Ivison R., 2004, ApJ, 611, 725
Blain A. W., Smail I., Ivison R. J., Kneib J.-P., Frayer D. T., 2002, Phys. Rep., 369, 111
Blake C., Pope A., Scott D., Mobasher B., 2006, MNRAS, 368, 732
Blanc G. A. et al., 2008, ApJ, 681, 1099
Bolzonella M., Miralles J.-M., Pelló R., 2000, A&A, 363, 476
Borys C., Chapman S., Halpern M., Scott D., 2003, MNRAS, 344, 385
Bothwell M. S. et al., 2010, MNRAS, 405, 219
Bower R. G., Benson A. J., Malbon R., Helly J. C., Frenk C. S., Baugh C. M., Cole S., Lacey C. G., 2006, MNRAS, 370, 645
Bower R. G., McCarthy I. G., Benson A. J., 2008, MNRAS, 390, 1399
Brodwin M. et al., 2008, ApJ, 687, L65
Brown M. J. I. et al., 2008, ApJ, 682, 937
Cappellari M. et al., 2011, MNRAS, 413, 813
Carrera F. J., Page M. J., Stevens J. A., Ivison R. J., Dwelly T., Ebrero J., Falocco S., 2011, MNRAS, 413, 2791
Chapman S. C., Blain A., Ibata R., Ivison R. J., Smail I., Morrison G., 2009, ApJ, 691, 560
Chapman S. C., Blain A. W., Ivison R. J., Smail I. R., 2003, Nature, 422, 695
Chapman S. C., Blain A. W., Smail I., Ivison R. J., 2005, ApJ, 622, 772
Ciotti L., Ostriker J. P., 2007, ApJ, 665, 1038
Ciotti L., Ostriker J. P., Proga D., 2010, ApJ, 717, 708
Coil A. L. et al., 2009, ApJ, 701, 1484
Coil A. L., Hennawi J. F., Newman J. A., Cooper M. C., Davis M., 2007, ApJ, 654, 115
Coil A. L. et al., 2008, ApJ, 672, 153
Conroy C., Wechsler R. H., 2009, ApJ, 696, 620
Cooray A. et al., 2010, A&A, 518, L22+
Coppin K. et al., 2006, MNRAS, 372, 1621
Coppin K. E. K. et al., 2008, MNRAS, 389, 45
Croom S. M. et al., 2005, MNRAS, 356, 415

Croom S. M., Schade D., Boyle B. J., Shanks T., Miller L., Smith R. J., 2004, ApJ, 606, 126

Croton D. J. et al., 2006, MNRAS, 365, 11

da Ângela J. et al., 2008, MNRAS, 383, 565

Damen M. et al., 2011, ApJ, 727, 1

Davé R., Finlator K., Oppenheimer B. D., Fardal M., Katz N., Kereš D., Weinberg D. H., 2010, MNRAS, 404, 1355

Decarli R., Falomo R., Treves A., Labita M., Kotilainen J. K., Scarpa R., 2010, MNRAS, 402, 2453

Di Matteo T., Springel V., Hernquist L., 2005, Nature, 433, 604

Donoso E., Li C., Kauffmann G., Best P. N., Heckman T. M., 2010, MNRAS, 407, 1078

Dunlop J. S., 2011, ASP Conf. Series in press (arXiv:1108.5679)

Eales S., Lilly S., Gear W., Dunne L., Bond J. R., Hammer F., Le Fèvre O., Crampton D., 1999, ApJ, 515, 518

Elbaz D. et al., 2011, A&A, 533, A119

Engel H. et al., 2010, ApJ, 724, 233

Estrada J., Sefusatti E., Frieman J. A., 2009, ApJ, 692, 265

Fakhouri O., Ma C.-P., Boylan-Kolchin M., 2010, MNRAS, 406, 2267

Feruglio C., Maiolino R., Piconcelli E., Menci N., Aussel H., Lamastra A., Fiore F., 2010, A&A, 518, L155+

Fine S., Croom S. M., Bland-Hawthorn J., Pimbblet K. A., Ross N. P., Schneider D. P., Shanks T., 2010, MNRAS, 409, 591

Fine S., Shanks T., Nikoloudakis N., Sawangwit U., 2011, MNRAS in press (arXiv:1107.5666)

Fischer J. et al., 2010, A&A, 518, L41

Gawiser E., Wolfe A. M., Prochaska J. X., Lanzetta K. M., Yahata N., Quirrenbach A., 2001, ApJ, 562, 628

Geach J. E., Smail I., Moran S. M., MacArthur L. A., Lagos C. d. P., Edge A. C., 2011, ApJ, 730, L19+

Gehrels N., 1986, ApJ, 303, 336

Genzel R. et al., 2008, ApJ, 687, 59

Gilli R. et al., 2007, A&A, 475, 83

—, 2009, A&A, 494, 33

Greene J. E., Zakamska N. L., Ho L. C., Barth A. J., 2011, ApJ, 732, 9

Greve T. R. et al., 2005, MNRAS, 359, 1165

Güsten R., Nyman L. Å., Schilke P., Menten K., Cesarsky C., Booth R., 2006, A&A, 454, L13

Hainline L. J., Blain A. W., Smail I., Alexander D. M., Armus L., Chapman S. C., Ivison R. J., 2011, ApJ, 740, 96

Hamana T., Ouchi M., Shimasaku K., Kayo I., Suto Y., 2004, MNRAS, 347, 813

Hickox R. C. et al., 2009, ApJ, 696, 891

—, 2011, ApJ, 731, 117

Hopkins P. F., Somerville R. S., Hernquist L., Cox T. J., Robertson B., Li Y., 2006, ApJ, 652, 864

Hughes D. H. et al., 1998, Nature, 394, 241

Ivison R. J., Papadopoulos P. P., Smail I., Greve T. R., Thomson A. P., Xilouris E. M., Chapman S. C., 2011, MNRAS, 412, 1913

Kaiser N., 1984, ApJ, 284, L9

Kauffmann G., Haehnelt M., 2000, MNRAS, 311, 576

Kelly B. C., Vestergaard M., Fan X., Hopkins P., Hernquist L., Siemiginowska A., 2010, ApJ, 719, 1315

Kim J., Edge A. C., Wake D. A., Stott J. P., 2011, MNRAS, 410, 241

Kollmeier J. A. et al., 2006, ApJ, 648, 128

Kotilainen J. K., Falomo R., Decarli R., Treves A., Uslenghi M., Scarpa R., 2009, ApJ, 703, 1663

Krumpe M., Miyaji T., Coil A. L., 2010, ApJ, 713, 558

Lacey C., Cole S., 1993, MNRAS, 262, 627

Lagos C. D. P., Baugh C. M., Lacey C. G., Benson A. J., Kim H.-S., Power C., 2011, MNRAS, 1776

Landy S. D., Szalay A. S., 1993, ApJ, 412, 64

Lauer T. R., Tremaine S., Richstone D., Faber S. M., 2007, ApJ, 670, 249

Le Floc'h E. et al., 2005, ApJ, 632, 169

Lee K.-S., Giavalisco M., Gnedin O. Y., Somerville R. S., Ferguson H. C., Dickinson M., Ouchi M., 2006, ApJ, 642, 63

Li C., Kauffmann G., Wang L., White S. D. M., Heckman T. M., Jing Y. P., 2006, MNRAS, 373, 457

Lindner R. R. et al., 2011, ApJ, 737, 83

Mandelbaum R., Li C., Kauffmann G., White S. D. M., 2009, MNRAS, 393, 377

Marconi A., Axon D. J., Maiolino R., Nagao T., Pastorini G., Pietrini P., Robinson A., Torricelli G., 2008, ApJ, 678, 693

Merloni A. et al., 2010, ApJ, 708, 137

Michałowski M. J., Dunlop J. S., Cirasuolo M., Hjorth J., Hayward C. C., Watson D., 2011, A&A submitted (arXiv:1108.6058)

Mihos J. C., Hernquist L., 1994, ApJ, 431, L9

Mo H. J., Mao S., White S. D. M., 1998, MNRAS, 295, 319

Myers A. D., Brunner R. J., Nichol R. C., Richards G. T., Schneider D. P., Bahcall N. A., 2007, ApJ, 658, 85

Myers A. D. et al., 2006, ApJ, 638, 622

Myers A. D., White M., Ball N. M., 2009, MNRAS, 399, 2279

Narayanan D., Hayward C. C., Cox T. J., Hernquist L., Jonsson P., Younger J. D., Groves B., 2010, MNRAS, 401, 1613

Nelan J. E., Smith R. J., Hudson M. J., Wegner G. A., Lucey J. R., Moore S. A. W., Quinney S. J., Suntzeff N. B., 2005, ApJ, 632, 137

Netzer H., Marziani P., 2010, ApJ, 724, 318

Norberg P., Baugh C. M., Gaztañaga E., Croton D. J., 2009, MNRAS, 396, 19

Overzier R. A., Röttgering H. J. A., Rengelink R. B., Wilman R. J., 2003, A&A, 405, 53

Page M. J., Stevens J. A., Ivison R. J., Carrera F. J., 2004, ApJ, 611, L85

Peebles P. J. E., 1993, Principles of physical cosmology. Princeton University Press, Princeton, NJ

Peterson B. M. et al., 2004, ApJ, 613, 682

Pope A. et al., 2008, ApJ, 675, 1171

Quadri R. et al., 2007, ApJ, 654, 138

Quadri R. F., Williams R. J., Lee K., Franx M., van Dokkum P., Brammer G. B., 2008, ApJ, 685, L1

Rafferty D. A., McNamara B. R., Nulsen P. E. J., 2008, ApJ, 687, 899

Richards G. T. et al., 2006, AJ, 131, 2766

Rodighiero G. et al., 2010, A&A, 515, A8+

Ross N. P. et al., 2009, ApJ, 697, 1634

Sanders D. B., Soifer B. T., Elias J. H., Madore B. F., Matthews K., Neugebauer G., Scoville N. Z., 1988, ApJ, 325, 74

Scott S. E. et al., 2002, MNRAS, 331, 817

Shen Y., Greene J. E., Strauss M. A., Richards G. T., Schneider D. P., 2008, ApJ, 680, 169

Shen Y., Kelly B. C., 2010, ApJ, 713, 41

Sheth R. K., Mo H. J., Tormen G., 2001, MNRAS, 323, 1

Siringo G. et al., 2009, A&A, 497, 945

Smail I., Ivison R. J., Blain A. W., 1997, ApJ, 490, L5

Smith R. E. et al., 2003, MNRAS, 341, 1311

Somerville R. S., Hopkins P. F., Cox T. J., Robertson B. E., Hernquist L., 2008, MNRAS, 391, 481

Springel V., Di Matteo T., Hernquist L., 2005, MNRAS, 361, 776

Starikova S. et al., 2011, ApJ, 741, 15

Stevens J. A., Page M. J., Ivison R. J., Carrera F. J., Mittaz J. P. D., Smail I., McHardy I. M., 2005, MNRAS, 360, 610

Stott J. P., Kim J., Edge A. C., Wake D. A. a., 2011, MNRAS submitted, 410, 241

Sturm E. et al., 2011, ApJ, 733, L16

Swinbank A. M., Chapman S. C., Smail I., Lindner C., Borys C., Blain A. W., Ivison R. J., Lewis G. F., 2006, MNRAS, 371, 465

Tacconi L. J. et al., 2010, Nature, 463, 781

—, 2008, ApJ, 680, 246

—, 2006, ApJ, 640, 228

Tempel E., Saar E., Liivamägi L. J., Tamm A., Einasto J., Einasto M., Müller V., 2011, A&A, 529, A53+

Tinker J., Kravtsov A. V., Klypin A., Abazajian K., Warren M., Yepes G., Gottlöber S., Holz D. E., 2008, ApJ, 688, 709

Tinker J. L., Wetzel A. R., 2010, ApJ, 719, 88

Vestergaard M., 2002, ApJ, 571, 733

Vestergaard M., Peterson B. M., 2006, ApJ, 641, 689

Wake D. A., Croom S. M., Sadler E. M., Johnston H. M., 2008a, MNRAS, 391, 1674

Wake D. A. et al., 2008b, MNRAS, 387, 1045

Wardlow J. L. et al., 2011, MNRAS, 415, 1479

Webb T. M. et al., 2003, ApJ, 582, 6

Weiß A. et al., 2009, ApJ, 707, 1201

Williams C. C. et al., 2011, ApJ, 733, 92

Xia J.-Q., Negrello M., Lapi A., De Zotti G., Danese L., Viel M., 2011, arXiv:1111.4212

Zehavi I. et al., 2011, ApJ, 736, 59

—, 2005, ApJ, 630, 1